High pressure adsorption of hydrogen sulfide and regeneration ability of ultra-stable Y zeolite for natural gas sweetening

Mehdi Rahmani[a], Babak Mokhtarani[a]*, Nejat Rahmanian[*b]

[a] *Chemistry and Chemical Engineering Research Center of Iran, P.O. Box 14335-186, Tehran 1496813151, Iran*

[b] *Department of Chemical Engineering, Faculty of Engineering and Informatics, University of Bradford, Bradford BD7 1DP, UK*

**Corresponding authors E-mail: mokhtaranib@ccerci.ac.ir Tel.: +98 21 44787770; Fax: +98 2144787781 and n.rahamnian@bradford.ac.uk(Tel.: +441274234552).*

Abstract:

Adsorbents are developing in the various separation industries; these adsorbents can use to sweeten natural gas and remove hydrogen sulfide. Many commercial adsorbents are not regenerable when exposed to hydrogen sulfide because hydrogen sulfide is highly reactive. For H_2S removal, the main challenge when using surface adsorbent, is the dissociation adsorption of H_2S and non-regenerability of adsorbent. In this study, ultra-stable Y (USY) zeolite, was chosen to adsorb hydrogen sulfide due to its unique physical and chemical properties. To accurately model the adsorption isotherms, experimental adsorption data were measured in high pressure up to 12 bar for hydrogen sulfide and 21 bar for carbon dioxide, methane, and nitrogen as other natural gas components. The experiments were performed at three temperatures of 283, 293 and 303 K. Toth model fitted the experimental data very well, and the capacity of hydrogen sulfide adsorption on USY at the temperature of 283 K and pressure of 12 bar is 4.47 mmol/g that is noticeable. By performing ten cycles of adsorption and regeneration of hydrogen sulfide on USY, the regenerability of the adsorbent was investigated and compared by conducting a similar test on commercial 13X adsorbent. USY is found to be completely regenerable when exposed to hydrogen sulfide. The isosteric adsorption heat of hydrogen sulfide on the adsorbent is 18.1 kJ/mol, which indicates physical adsorption, and the order of adsorption capacity of tested compounds on USY is $H_2S>CO_2>>CH_4>N_2$.

Keywords: ultra-stable Y zeolite, hydrogen sulfide adsorption, regenerability, natural gas sweetening.

1. Introduction

Surface adsorbents, especially zeolites as molecular sieves, are increasingly expanding in various separation industries. In the recent years in natural gas industries, zeolite adsorbents have been broadened in liquefied petroleum gas treatment, ethane treatment, dehydration, nitrogen production, etc. Hydrogen sulfide removal from natural gas, although research is carried out on surface adsorbents, they have not yet been used extensively and industrially. Conventional commercial surface adsorbents such as activated carbon and commercial zeolites like FAU and LTA type are faced with challenges of non-regenerability and structure destruction in the exposure to highly active hydrogen sulfide gas [1–3]. This study is concerned with a cost-effective, stable, and regenerable adsorbent for natural gas sweetening.

In this study, the adsorption of hydrogen sulfide, methane, carbon dioxide, and nitrogen as natural gas components were investigated on ultra-stable Y (USY) zeolite, which includes the capacity of adsorption, heat of adsorption, regenerability, and selectivity. The promising results of this study suggest USY can be used in natural gas sweetening. Currently, amine processes are the most common processes for removing hydrogen sulfide and carbon dioxide from natural gas [4]. However, the current focus of researchers is to find new gas-sweetening methods that have lower fixed and operating costs and also are effective in the field of health, safety and environment [5]. Conventional zeolites in industries such as FAU (13X) and LTA (4A, 5A), when faced with sour gas containing hydrogen sulfide, perform dissociation adsorption, which is irreversible and non-regenerable [6–12]. There are a limited number of studies have been conducted on this issue. This is mainly due to the enormous hazards of hydrogen sulfide and the severe lethality of this gas and such the available studies have been operated at low concentrations of hydrogen sulfide or low pressures close to the atmosphere, which makes it challenging to find the appropriate adsorption behavior. To correctly measure the adsorption behavior of zeolites, it is necessary to calculate adsorption isotherms at high pressures and high concentrations. In this case, a better adsorption model coordinates with the experimental data, and the rest of the calculations, such as the heat of adsorption, will be more accurate. To check the chemical reaction of the adsorbent lattice towards hydrogen sulfide gas, the entire network must be affected by high gas concentration. Most of the available studies in the literature have focused on the adsorption capacity of adsorbents for natural gas sweetening while there is a lack of information and studies in the field of adsorbent regenerability [13]. This study was conducted at high pressure and focused on regenerability with completely repeatable results. Our goals in this study are to find adsorption capacity, calculate the isosteric enthalpy of adsorption, adsorbent regenerability and the ideal selectivity of the USY to natural gas sweetening.

Hydrogen sulfide is highly active and destroys many structures. To find the reasons for zeolite's non-regenerability, and destruction of their structure, various theories have been expressed that the zeolite's lattice bond is broken, and the SiOHAl bond is formed [7,9]. In another study, the acid-base character and the partial charge of oxygen (δ_o) in the zeolitic structure have been investigated, and dissociative adsorption has been attributed to these evidences [11]. In some other studies, the dissociation adsorption of hydrogen sulfide on zeolites is considered due to adsorption-redox processes [14], and they have defined the retention mechanism [6].

Ultra-stable Y zeolite is a stable catalyst against acid, so it can be suitable for adsorbing hydrogen sulfide from natural gas with acidic properties. USY shows thermal and hydrothermal stability, this adsorbent is produced by a current with a high temperature of 773 Kelvin; during this process, aluminium cations are removed from the lattice of zeolite and in this way, the structure of zeolite is stabilized [15]. It is expected that with the removal of more aluminium cations and the increase in the ratio of Si/Al, no more dissociation adsorption will occur, and the adsorbent will be regenerable [9,16].

In this research, the equilibrium adsorption of hydrogen sulfide up to 12 bar[1] and carbon dioxide, methane, and nitrogen as compounds present in the natural gas were measured up to 21 bar. After finding the adsorption isotherms at high pressures, the appropriate adsorption model was selected with an excellent fit to the experimental data. With the accurate model obtained from the experimental data, the heat of adsorption and the ideal selectivity was calculated to find the adsorption behavior, which will be discussed in detail in the next section.

Regarding hydrogen sulfide adsorption on USY zeolite, no published data were found for comparison. Few studies have also been published regarding the static adsorption of hydrogen sulfide on Y zeolites. It should be noted that Y zeolite is very different from USY in terms of Si/Al ratio. In a study at a very low relative pressure of 0.005 bar at 298 K, the hydrogen sulfide adsorption isotherm on NaY zeolite was calculated, and the final adsorption capacity was published to be 4.7 mmol/g according to Dubinin-Astakhov's model [17]. In another study, the adsorption capacity of 2.25 mmol/g was reported at a low H_2S concentration of 90 ppm on CuY and AgY. It has also been shown that these sorbents are not regenerable in common physical regeneration processes [18]. The adsorption of H_2S on NaY zeolite was studied in equilibrium up to a relative pressure of 1.2 bar of H_2S, and the maximum adsorption capacity is higher than 6.0 mmol/g. Desorption curves show the residual effect related to the chemical adsorption of H_2S on the zeolite surface [19].

Limited efforts have been made to calculate hydrogen sulfide adsorption isotherms on Y zeolites, which again were also measured at low pressure and concentration. In this study, the adsorption of pure hydrogen sulfide on USY zeolite at three different temperatures of 283, 293, and 303 K up to 12 bar is calculated, and the adsorption isotherms are presented. The adsorption of hydrogen sulfide on this zeolite at 12 bar is 4.47, 4.07, and 3.72 mmol/g at temperatures of 283, 293, and 303 K, respectively. The results show that this gas has good adsorption on USY. Table 1 compares the capacity of hydrogen sulfide adsorption on different zeolite adsorbents. For more details, review articles can be used to compare with other surface adsorbents [1,13,20,21].

[1] All pressure units are absolute bar

Table 1: Adsorption of hydrogen sulfide on different zeolitic adsorbents

Adsorption isotherms of other natural gas components up to 21 bar were measured and modelled at temperatures of 283, 293, and 303 K, which are: A) Carbon dioxide; due to its kinetic diameter and polarity, is considered the main competitor of hydrogen sulfide in the adsorption process, this gas is associated with hydrogen sulfide in sour gas storage. B) Methane gas; is a component that has the highest molar percentage in natural gas. C) Nitrogen is a gas that acts like an inert gas under normal conditions of temperature and pressure and is usually present in natural gas. The tested gases are pure, and the pressures are considered high enough to obtain accurate models. Temperatures are chosen with a difference of 10 K to calculate the heat of adsorption accurately [29–31]. In the end, the ideal selectivity was investigated, and the regeneration of the adsorbent was checked to get a comprehensive view of acid gas adsorption by USY.

2. Experimental Section

2.1. Materials

USY zeolite was purchased from Fuyo Company, it is a high silica ultra-stable zeolite; Zeolite 13X was prepared from Hengye Inc. Other tested gases include a) nitrogen gas, purity: 0.9999; b) methane gas, purity: 0.9999; c) hydrogen sulfide gas, purity: 0.999; d) carbon dioxide gas, purity: 0.9995.

2.2. Apparatus and Sample Preparation

An apparatus was built to measure equilibrium adsorption isotherms by the volumetric method. The details of the apparatus, and adsorption isotherms measurements, have been described in our previous work on High-Silica ZSM-5 [22]. In this setup, temperature and pressure sensors for the gas storage cylinder and temperature and pressure sensors for the reactor are used with a measurement accuracy of 1 mbar and 0.1 K. The volume of the gas storage cylinder is constant, so the amount of gas injected into the reactor is determined by the pressure and temperature and proper equations of state. By checking the pressure of the reactor, which is kept at a constant temperature with a specific volume, the amount of gas adsorption in each equilibrium stage is calculated. Finally, the equilibrium adsorption amount is obtained for different pressures, and the adsorption isotherm curves are drawn.

Adsorption isotherms are generally measured by three techniques: chromatographic, gravimetric and volumetric. In this study, the volumetric method was used. Simply with a valve, some of the adsorbates enters the reactor and the final equilibrium pressure is calculated. Therefore, by knowing the type of gas, volume, pressure and temperature of the gas storage cylinder and the reactor and choosing the appropriate equation of state, the adsorption amount of the substance on the adsorbent is calculated. This widely used method is effective, and absolute adsorption can be measured with good accuracy [32]. The temperature and pressure are calculated by accurate sensors, so before doing the adsorption calculations, the volume of the gas storage cylinder and the reactor containing the adsorbent needs to be calculated. The volume of the injection cylinder, which has no adsorption, is measured several times by various light and heavy gases with a certain weight, such as CO_2, CH_4, N_2 and He. The free volume of the reactor containing the adsorbent is also calculated by helium gas as a molecular probe, which is a well-known method [32]. At low helium pressures, the amount of adsorption on the adsorbent is negligible, and the volume of the adsorption reactor is calculated without considering the adsorbent. By knowing the temperature, pressure and volume of the reactor and choosing an appropriate equation of state for each gas, the number of remaining moles in the reactor is calculated. Finally, the mole adsorbed on the adsorbent is calculated according to the following equation.

$$n_{ads} = n_T - n_{eq} \qquad (1)$$

where n_{ads} is adsorbed moles, the n_T is injected mol and n_{eq} is the remaining moles of the gas in the reactor. An interactive software [33] is used to calculate thermodynamic properties, which includes accurate equations of state for hydrogen sulfide [34], carbon dioxide [35], methane [36], nitrogen [37] and helium [38].

The air around us contains water vapor and carbon dioxide, which are adsorbed in the adsorbent. To ensure that waste materials are not left in the molecular sieve, the adsorbent is heated to a temperature of 570 K at a rate of 2 K/min and then remains at this temperature for an hour; when the zeolites are still at their temperature, the adsorbent is entered into the reactor with safety equipment, and the adsorption bed is immediately evacuated under vacuum and prepared for testing. This process is similar to the calcination process, although the zeolite had already been calcined.

Theoretically, experimental errors are the difference between actual and measured values, these errors can be positive or negative. The real value is never known, so one of the characteristics of experimental data is the measurement of uncertainty. Both systematic and random uncertainties exist in all cases, and the true value is essentially within a certain range, it should be ensured that the uncertainties are small enough [39]. Determining the uncertainties created by the sensors is not a difficult task, can be calculated with a normal distribution, and in most cases, these values are provided by the sensor manufacturers. In experimental studies, generally, the calculated values are not direct measurements, and a value is calculated based on different parameters with a relationship. Uncertainty calculation based on direct equipment errors is called indirect uncertainty [40]. In this study, a temperature sensor was used, with a 0.1 K error, and pressure sensors also have an error of 1 mbar. Temperature and pressure are needed to calculate density, which is directly related to pressure and inversely related to temperature, therefore, knowing the direct error of the sensors, the uncertainties have been calculated indirectly by the derivation method [40].

2.3. Adsorption Modeling.

Adsorption data on USY were fitted to Langmuir and Freundlich isotherm models as base models and Sips and Toth as well-known models derived from the base models. Langmuir and Freundlich's isotherms include two parameters while Sips and Toth consist of three parameters; Sips and Toth models can characterize the laboratory information better than other two-parameter models [41]. Through fitting the empirical data, adsorption isotherms were calculated with the mentioned models with 95% confidence.

The Langmuir adsorption isotherm assumes that adsorption takes place homogeneously in certain sites. Langmuir was the first to present a coherent adsorption theory on a flat surface based on the kinetic point of view[42]. The Langmuir equation is as follows:

$$q = \frac{q_m bP}{1 + bP} \qquad (2)$$

The maximum adsorption on the adsorbent surface is represented as q_m in terms of mmol/g, and b is the binding affinity. According to the Langmuir equation, if P enhances infinite, the whole capacity of the monolayer will be complete.

Freundlich isotherm is one of the first empirical equations to describe equilibrium data and is used to characterize heterogeneous systems. This equation deals with the exponential distribution of active sites and their energies by defining surface heterogeneity [41]. The Freundlich equation is written as follows

$$q = k_F P^{1/n} \qquad (3)$$

the driving force of interactions expressed by n that is a constant, and k_F is the Freundlich constant.

The Sips adsorption isotherm is a well-known adsorption model. This model is a combination of Freundlich and Langmuir models and is as follows [41]

$$q = \frac{q_m (bp)^{1/n}}{1+(bp)^{1/n}} \qquad (4)$$

Maximum adsorption, like the Langmuir equation, is displayed by q_m in terms of mmol/g, the Freundlich constant is shown by n, and b is the Langmuir constant, which is related to the adsorption site's energy.

The Toth isotherm model is an empirical equation, built up to increase the accuracy of the Langmuir isotherm. It is a useful model to describe homogeneous and heterogeneous adsorption systems and is commonly used; this model is as below

$$q = \frac{q_m bP}{[1+(bp)^t]^{1/t}} \qquad (5)$$

t is the Toth constant, b is adsorption affinity, and the maximum adsorption capacity is denoted by q_m [42].

To understand how the experimental data are fitted on the models, a detailed statistical analysis is required. In this article, to compare and select the best model, statistical analysis of Standard Error, r, R^2, and AICc were calculated. There are other statistical analysis methods such as Sum Square of Errors (ERRSQ), Standard Error, Hybrid Fractional Error Function (HYBRID), Average Relative Error (ARE), Sum of Absolute Errors (EABS), and Marquardt's Percent Standard Deviation (MPSD); in our opinion, Akaike Information Criterion (AIC) is a very effective mixed model that can express the difference between various curve fitting numerically [43]. The best curve-fitting model may need to be selected from several closely related options; therefore, there is a useful numerical index, called AIC. The more negative the number, the more accurate the curve-fitting of the experimental data. AIC as a mathematical method quantitatively measures the fit of a model to the data. AICc is a modified model of AIC, corrected for small sample sizes [44,45].

2.4. Isosteric Enthalpy of Adsorption

Adsorption on the adsorbent surface causes heat, increase in temperature affects the adsorption. Isosteric heat of adsorption is used to interpret the behavior of the adsorbate-adsorbent. The isosteric heat of adsorption, as seen in equation (6), thermodynamically is the difference between the gas molar enthalpy and the ratio of the tiny change in the enthalpy of adsorption to the infinitesimal change in the amount of adsorption.

$$q_{st} = h_g - [\frac{\partial H^E}{\partial n^E}]_T \qquad (6)$$

n^E is the adsorption amount in terms of (mol/g), and H^E is the specific enthalpy, expressed in terms of (J/g). To simplify equation (6), we use one of the famous methods called the Clausius-Clapeyron relation, which is for a one-component system. Clausius- Clapeyron relation is as follows:

$$q_{st} = -R.[\frac{\partial lnP}{\partial (1/T)}]_{n^E} \qquad (7)$$

Using a set of adsorption isotherms at several temperatures, the heat of adsorption can be obtained as a linear regression of lnP versus $1/T$ at constant coverage fraction (n^E) [29,31]. Isosteric heat of adsorption (q_{st}) is the equal negative enthalpy of adsorption ($q_{st} = -\Delta H$) and the negative enthalpy change means that heat is released from the adsorption process. q_{st} is a positive quantity, experimentally can be calculated from a set of isotherms that are measured at close but different temperatures [46]. The isosteric heat of adsorption is a valuable and widely used figure that indicates the strength of binding interactions at fixed temperature, pressure, and coverage [47].

3. Results and Discussion

3.1. Characterization of physical properties

Energy Dispersive X-Ray Analysis (EDAX) test with Scanning Electron Microscopy (SEM) (FEI Quanta 400) was used to determine the zeolite composition. EDAX analysis or EDS is an add-on to SEM devices to determine the percentage of elements in solid samples. This analysis can identify the type of element and its weight or atomic percentage by using the unique X-ray energy emitted from the sample. The USY surface image is shown in Figure 1. The surface roughness of pristine adsorbent with regular morphology of the structure can be seen in the SEM image, and crystal size distribution appears to be uniform.

Figure 2 shows the distribution of different atoms that make up the aluminosilicate structure of the zeolite. X-ray elemental mapping shows Al and Si atoms are homogeneously dispersed on the surface; a uniform distribution of sodium is observed in the aluminosilicate network.

Figure 1: SEM image of USY surface.

Figure 2: scattering of Na, Si, Al, and O atoms

The weight percentage of constituent elements of the tested USY zeolite is given in Table 2. The weight ratio of Si/Al is equal to 54.7.

Table 2: weight percentage of the constituent elements of USY

Among the methods used to determine porosity, the BET method, which is based on adsorption, has received much attention. In this method, a complete layer of adsorbed substance molecules is formed on the surface. By knowing the average thickness of a molecule, it is possible to calculate the surface occupied by a molecule and measure the total surface area of the USY. Based on the BET theory as well as the measured adsorption and desorption values of the adsorbate, this system can calculate the specific surface area, diameter, volume and size distribution of the pores. BET analysis on USY was performed based on measuring the volume of nitrogen gas adsorbed and desorbed at a constant temperature of liquid nitrogen (77 Kelvin). In the BET test, after the cell containing the desired sample is placed in the liquid nitrogen tank, the amount of gas adsorbed is calculated by gradually increasing the nitrogen gas pressure in 28 steps. Then, by gradually decreasing the gas pressure, the amount of desorption is measured and finally, the graph of the volume of nitrogen gas adsorbed and desorbed by the USY is drawn.

Figure 3: Adsorption-Desorption isotherm of nitrogen on the USY; circles, adsorption; squares, desorption.

The adsorption and desorption of nitrogen by USY are shown in Figure 3. The BET (C) constant is 975, which is high and indicates that this adsorbent is microporous. The adsorbent is the IV type, and hysteresis loop type H3 is observed according to the IUPAC classification. The amount of adsorbent surface was obtained by the slope and y-intercept on the adsorption graph. the volume of the micropore was 0.24 cm3/g, by t-plot analysis with an Intercept of 155.07; which is 0.58 of the total volume. In Figure 4, the size distribution of the pores can be seen based on the BJH method, the peak of which is 1.64 nm. The total results of the surface analysis of USY are shown in Table 3.

Figure 4: Pore size distribution of USY

Table 3: Specifications of ultra-stable Y Zeolite

3.2. Adsorption Isotherms Measurement

The equilibrium adsorption of hydrogen sulfide, methane, carbon dioxide and nitrogen was measured to investigate, how natural gas components adsorb on USY; especially the difference between the adsorption of hydrogen sulfide and carbon dioxide was determined as they compete for adsorption. The investigated pressure for hydrogen sulfide is up to 12 bar and for the rest of the compounds up to 20 bar. Adsorption isotherms were measured at three different temperatures; the difference between tested temperatures is 10K; at temperatures of 283, 293, and 303 K, per increase in absolute pressure in terms of bar, the capacity of adsorption is reported as $q/(mmol_{adsorbate}/g_{adsorbent})$. The experimental data were fitted to four well-known isotherm models, and statistical analysis of the data fitting for each component and temperature was presented according to Table 4 collectively. To better see the trend of the isotherms, the adsorption isotherm of the Toth model was illustrated in graphs, which fits well with the experimental data.

Table 4: The statistical model of data fitting

Hydrogen sulfide adsorption isotherms were measured at more than 12 bar and are shown in Figure 5. Maximum adsorption at 12 bar and temperature of 283 K is 4.47 mmol/g, this value is 4.07 and 3.72 mmol/g for temperatures of 293 and 303 K, respectively. Toth and Sips models have acceptable answers according to statistical analysis (Table 4). Toth's model is fitted to the experimental data and shown with dashed lines. The data fit on Langmuir and Freundlich models is not as good as other models. The experimental data obtained from the volumetric tests at three different temperatures are shown in Table 5, this information is the basis for the modelling of the adsorption process.

Figure 5: H_2S adsorption isotherms on USY; blue tilted squares, 283K; red circles, 293K; green triangles, 303K; dashed lines, Toth model.

Table 5: Experimental data of H2S adsorption on USY

Kinetic diameter and polarity are the main factors affecting adsorption, and these factors cause competition in adsorption for carbon dioxide and hydrogen sulfide [48]. Carbon dioxide is present in natural gas along with hydrogen sulfide, so it needs to be checked for competitive adsorption. Carbon dioxide adsorption capacity on USY at three temperatures of 283, 293, and 303 K and 12 bar are 3.93, 3.54, and 3.01 mmol/g. Carbon dioxide adsorption isotherms that have lower risks than hydrogen sulfide, were figured out up to 21 bar and are illustrated in Figure 6. Under the various statistical analysis that is available in Table 4, the Toth and Sips models fit better than the rest of the adsorption models on the experimental results. Toth model is shown as dashed lines in Figure 6 to see the trend of carbon dioxide adsorption.

Figure 6: CO_2 adsorption isotherms on USY; blue tilted squares, 283K; red circles, 293K; green triangles, 303K; dashed lines, Toth model.

Methane gas has a major portion in natural gas, so investigating isotherms of this gas on zeolite is important for natural gas sweetening. The static isotherms of methane adsorption on USY zeolite were investigated up to 21 bar as illustrated in Figure 7. The statistical analysis (Table 4) shows that the models of Toth, Sips, and Langmuir fit well with this information and can be used with good accuracy. In Figure 7, Toth's model for the isotherms is shown as a dashed line.

Figure 7: Methane adsorption isotherms on USY; blue tilted squares, 283K; red circles, 293K; green triangles, 303K; dashed lines, Toth model.

The experimental isotherms of nitrogen adsorption were plotted in Figure 8 at three different temperatures; the obtained experimental data were calculated up to a pressure of 21 bar and fitted with models. All four models have almost good results. In the figure, the Toth model is shown with a dashed line.

Figure 8: Nitrogen adsorption isotherms on USY; blue tilted squares, 283K; red circles, 293K; green triangles, 303K; dashed lines, Toth model.

The experimental data of carbon dioxide, methane and nitrogen adsorption are given in Table 6 for comparison, because the measurement scale is up to 21,000 millibars, the use of this table is useful for better visibility of the obtained experimental results. To show the difference between the adsorption of compounds by USY, all the adsorption isotherms were displayed in Figure 9 at 283 K. As shown, the hydrogen sulfide adsorption capacity of USY is the highest, followed by carbon dioxide, methane, and nitrogen respectively. At different pressures, the adsorption capacity of hydrogen sulfide and carbon dioxide are much more different than methane and nitrogen; this phenomenon was not seen for High-Silica ZSM-5 [22], by calculating the heat of adsorption and the ideal selectivity in sections 3.3 and 3.5, we will have a better comparison.

Figure 9: Adsorption isotherms on USY at 283K; red circles, H_2S; green squares, CO_2; orange triangles, CH_4; blue tilted squares, N_2; dashed line, Toth model.

Table 6: Experimental data of CO_2, CH_4 and N_2 adsorption on USY

According to the statistical analysis for H_2S and CO_2 adsorption on USY (see Table 4), Langmuir and Freundlich's models do not fit well compared to Toth and Sips' models, but for CH_4 and N_2, the behavior changes. If the AICc analysis is examined to summarize the differences as a numerical index, it can be seen that for CH_4 and N_2, the numerical value of the Langmuir and Freundlich models has also been increased; in the case of nitrogen, it is close to the Toth and Sips models. We found that the Toth and Sips models are three parameters and can better support the experimental results; whereas the theoretical basis of these two models are the Langmuir and Freundlich models, which themselves have two parameters [41]; The reason is that, as shown in nitrogen and methane adsorption isotherms, the adsorption capacity is very low, and unlike the other two substances (H_2S and CO_2), the charts have not yet reached the saturation point, so the graphs are sub-saturation. Freundlich isotherm considers an exponential distribution for adsorption sites, which have a good prediction in the sub-saturation state. For the saturation state, the answer of Freundlich is not satisfactory [49]. Sips and Toth isotherms have shown reasonable matches to the experimental data, but if an isotherm is in the sub-saturation and a wide range of pressure is not considered, Sips and Toth can have errors in predicting the maximum adsorption; even if the data fit well at low pressures. This analysis is available in studies of adsorption isotherms [50].

If the Toth model is used, the exact adsorption heat is calculated at zero coverage, and if the Sips model is used, the adsorption heat of fractional loading of 0.5 should be the heat calculation criterion [41]. In both of these models, if the data are well-fitted, they have close heat of adsorption at the mentioned coverage; in fact, the limit of Henry's law does not consider in the Sips model, while the Toth model has this limitation and can use in low coverage [41]. From the investigated adsorption models, we noticed that the maximum adsorption (q_m) is well predicted for hydrogen sulfide and carbon dioxide, but not for nitrogen and methane. We do not have the correct maximum adsorption of methane and nitrogen (q_m) so cannot calculate half of it; therefore, we use the Toth model which is proper for the low coverage. Data fitting of the Toth model has given good answers, this model is suitable for both saturation and sub-saturation. To better interpret the results, and find out how the tested components are adsorbed on USY, the Toth model was chosen for all the adsorbates; so that the parameters of this model can be compared and analyzed together. These parameters are listed in Table 7. According to the above explanation, maximum adsorption capacity (q_m) for nitrogen and methane is not the criterion of our interpretations, and the adsorption capacity, selectivity and heat of adsorption of components on adsorbent are examined.

Factor b in the Toth model indicates binding affinity. The surface of the adsorbent is occupied by the adsorbate. In the binding sites, competition occurs, and b represents the interaction between the adsorbent and adsorbate. A larger b indicates a greater affinity of the adsorbate to be adsorbed and shows a higher activity in the adsorbent's free and bound site; in fact, it has a higher mean binding energy. t parameter is called Toth heterogeneity; when t is close to the unity, it indicates the homogeneity of the adsorbent; by decreasing the t, the mean binding energy also decreases [49,51].

Table 7: Toth model parameters, Henry's constant (K_H)

According to Table 7, the adsorption affinity for hydrogen sulfide (b) is higher than carbon dioxide, which indicates the higher adsorption affinity of hydrogen sulfide than carbon dioxide. The value of b for hydrogen sulfide and carbon dioxide is significantly higher than methane and nitrogen, which shows they have a higher interaction force. The conformity of the b factor and the adsorption capacity can also be seen in Figure 9. This figure shows the adsorption of all compounds on USY. It is clear that in different pressures up to 12 bar, the adsorption of hydrogen sulfide is more than carbon dioxide, and these two are significantly more than methane and nitrogen, while the difference between methane and nitrogen is less.

The value of the t parameter for all the tested components is very different from one, which shows that the adsorption on this adsorbent is heterogeneous. From hydrogen sulfide, carbon dioxide, methane, and nitrogen, respectively, the t number decreases, which indicates that the mean binding energy between the adsorbent and the adsorbate decreases and is consistent with the changes of the b factor. b shows the adsorption sites for the adsorbed molecule, and t represents the mean binding energy[49]; a higher mix of b and t, indicates a much greater affinity of the adsorbent for the adsorbate.

3.3. Heat of Adsorption

Two factors are usually more important to investigate the adsorption behavior of surface adsorbents, adsorption isotherm and heat of adsorption. The capacity of the adsorbent is studied with the adsorption isotherms, and the strength of the interaction between the adsorbent and adsorbate is investigated by the heat of adsorption. Theoretically, the heat of adsorption in homogeneous porous materials is constant and does not change with the change of loading; in fact, the mobility of molecules does not affect the surface interaction. In heterogeneous surfaces, molecules prefer to adsorb in the place that has the highest adsorption energy; at the beginning of adsorption in these sorbents, when the concentration is low, the heat of adsorption is higher; after that, by increasing the amount of adsorbate, molecules adsorb in the sites with lower energy, and the heat of adsorption decreases. The isosteric heat of adsorption (q_{st}) is the small change in the enthalpy of adsorption compared to the slight change in the amount of adsorption. Isosteric heat of adsorption is considered independent of temperature, and an average temperature is considered for it in the calculations [41]. If we use three adsorption isotherms to calculate the heat of adsorption, the average temperature is as follows.

$$T_{avg} = \frac{3}{\left(\frac{1}{T_1} + \frac{1}{T_2} + \frac{1}{T_3}\right)} \qquad (8)$$

To make the calculations of adsorption heat more accurate, three isotherms were investigated at an average temperature of 293 K and a temperature difference of 10 K. Two isotherms with a temperature difference of 20 K can also be used, but the answers are more reliable with three isotherms[29].

According to the isosteric heat of adsorption equation and Toth's model, the heat of adsorption can be calculated in different loadings according to equation (7) from linear regression of lnP versus $1/T$. The adsorption heat of hydrogen sulfide, methane, carbon dioxide, and nitrogen on USY zeolite were calculated and are given in Table 8; these are adsorption heat at zero loading.

Table 8: the heat of adsorption on USY

Figure 10: The trend of isosteric adsorption heat of CO_2, H_2S, CH_4 and N_2 on USY.

Figure 10 shows the trend of isosteric adsorption heat at different loadings for hydrogen sulfide, carbon dioxide, methane and nitrogen compounds. The trend of adsorption heat is almost constant and does not face a significant decrease at the beginning of loading, which indicates that the adsorption sites on the USY surface have uniform energy. Generally, if the adsorbent surface is energetically uniform, the heat of adsorption remains constant in different loads [42]. It is expected that the high-energy sites are first occupied by the adsorbent, and then the remaining sites are filled, which did not happen in this adsorbent. The concept of high-energy sites is relative but always contributes to the adsorption process unless the surface is energetically homogeneous. These energetic sites arise for different reasons, including functional groups, chemical elements on the surface, defects on the adsorbent surface, etc. [52] Adsorption heat can be divided into three categories a) Fluid–solid interaction heat (q_{f-s}), b) Fluid–fluid interaction heat (q_{f-f}) and c) Fluid–high-energy site interaction heat (q_{f-HES}) [52]. If the adsorbent has low polarity or the density of high-energy sites is low, the heat generated from these sites (q_{f-HES}) will be significantly reduced. hydrogen sulfide, carbon dioxide, methane and nitrogen have completely different polarities, but the adsorption heat does not drop at the beginning of loading for all four materials which indicates, q_{f-HES} is not present in this adsorbent and the adsorption heat is caused by q_{f-s} and q_{f-f}. Generally, with the increase in loading, q_{f-f} increases with a small rate at first and q_{f-s} decreases slightly [53]. For nitrogen and methane, with increasing loading, the amount of adsorption heat, increases slightly, which indicates the greater effect of q_{f-f}. The trend of adsorption heat in hydrogen sulfide and carbon dioxide is almost constant, which is influenced by q_{f-s} and q_{f-f}, therefore, the partial reduction of q_{f-s} is neutralized by q_{f-f}. The increase in heat of adsorption at the end of loading is also generally due to the interaction between molecules and the effect of condensation enthalpy [52].

One of the objectives of this study was to whether USY zeolite has physical or chemical adsorption when exposed to hydrogen sulfide, whether is it regenerable, or whether dissociation adsorption occurs. the performed tests are completely repeatable, and the calculated heat of adsorption indicates the physical adsorption of all tested gases, including hydrogen sulfide. It has been found that the hydrogen sulfide adsorption mechanism on USY is physical, and it is an outstanding achievement; Many commercial surface adsorbents have dissociative adsorption. The difference between physical and chemical adsorption depends on the surface forces of adsorption. In physical adsorption, intermolecular forces are the weak van der Waals type, while in chemical adsorption, a bond occurs with electrons movement, and bonds are stronger. In general, the heat of adsorption below 40 kJ/mol is considered physical; in some studies, up to 80 kJ/mol is also regarded as physical [54]. The adsorption heat obtained in this study is far less than these limits. In section 3.4, physical adsorption is checked, and the regenerability of this adsorbent will be explained in detail.

3.4. Regenerability of USY

To use an adsorbent industrially, the main selection factors are a) high adsorption capacity, b) suitable rate of adsorption, c) applicable mechanical properties, and d) stable chemical structure and regenerability. For an industrial adsorbent that is charged by performing cost and time-consuming operations, it should be possible to use it many times in the adsorption and regeneration cycles. Destruction of the adsorbent lattice, as well as the destruction of the binder during the adsorption and regeneration operations, reduces the performance of the molecular sieve and can lead to the pulverization of the molecular sieve particles and damage the downstream equipment even with proper filtering.

There is various surface adsorbent for adsorbing hydrogen sulfides, such as Metal-organic frameworks (MOFs), activated carbons, metal oxides, and zeolites. MOFs are expensive and do not yet have economic justification for removing hydrogen sulfide. Activated carbons show very good adsorption in confronting with hydrogen sulfide (more than 8 mmol/g[55]), but activated carbons have problems with regeneration, and the adsorption of hydrogen sulfide on them is chemisorption [13]. The adsorbent structure must be maintained during adsorption cycles. Metal oxide adsorbents are generally based on zinc, iron, and manganese, and have high adsorption at first, and then it decreases; because they have chemical adsorption. In addition, oxygen should be used to regenerate them, which produces sulfur dioxide [56]. Zeolites have a stable structure and can selectively remove various compounds. Because hydrogen sulfide is a polar compound, theoretically, it can be well adsorbed on zeolites and has selectivity over other natural gas components, but conventional industrial zeolites such as FAU (13X) and LTA (4A,5A) demonstrate dissociative adsorption in confronting with hydrogen sulfide, similar to the problem of activated carbons. Due to the high activity of hydrogen sulfide gas, dissociative adsorption occurs on some zeolites and causes the capacity of the zeolitic adsorbent to decrease over time.

In a study, LTA zeolite type 4A has been investigated for hydrogen sulfide adsorption; after five cycles of adsorption and regeneration, the adsorption has decreased to one-third of the initial adsorption amount, which is due to the dissociative adsorption of hydrogen sulfide by this adsorbent [57]. In another study, Sapo-43 was investigated; the regenerability of this adsorbent is suitable for water vapor, but it is non-regenerable in confronting hydrogen sulfide [24].

This study is related to an FAU-type adsorbent; a few articles have been published on the behavior of the FAU-type adsorbent when adsorbing hydrogen sulfide. In a study, Y-type zeolite with copper and silver ions in low concentration has been investigated, which shows that this adsorbent is not regenerable and only 69% of the adsorbed H_2S is released at a temperature above 723 K[18]. In another study on Y-type zeolite, an item called Δq_{eq} is defined, and with this item, is shown that due to the dissociative adsorption of hydrogen sulfide on Y zeolite, some of the adsorbed molecules are not desorbed. The adsorption heat of hydrogen sulfide was reported as 42 kJ/mol, which indicates a strong adsorbent-adsorbate interaction [19], this heat of adsorption is significantly different from our study on USY (18.1 kJ/mol).

To find the reason for the dissociative adsorption of hydrogen sulfide on zeolites, two findings are expressed; the much-cited study by Karge et al. with the IR method investigated the formed bonds when hydrogen sulfide adsorbed on aluminosilicate zeolite. It is shown that H_2S is converted to $H^{+} and\ SH^{-}$, and the proton attacks the zeolitic lattice and forms the Si-OH bond, and the structure is destroyed [9,58]. Following this study, other researchers investigated the adsorption behavior of zeolites towards hydrogen sulfide with IR and NMR spectroscopies on NaY zeolite. Both techniques have shown the dissociative adsorption of hydrogen sulfide, and it has been stated that Si-OH-Al bonds are formed in the adsorbent, which causes chemical adsorption, destruction of the zeolite structure, and non-regenerability [7]. Adsorption of hydrogen sulfide on zeolite 13X as another type of FAU zeolite has also been investigated;

it is found that dissociative adsorption has occurred, elemental sulfur is formed on the adsorbent surface, and a retention mechanism has been considered and published for this type of reaction [6,14].

Most of the mentioned studies have been investigated either in low concentrations of hydrogen sulfide mixed with another inert gas or at very low pressures. We decided to use pure hydrogen sulfide gas at high pressure so that all the adsorbent cavities were exposed to hydrogen sulfide for a long time. The hydrogen sulfide adsorption and desorption test were performed cyclically on this zeolite. With this method, the zeolite was loaded at the equilibrium pressure of 3 absolute bar, and after reaching the equilibrium, it was regenerated at the full vacuum pressure until the vacuum was maintained, and there was no more desorption gas. Ten cycles of adsorption and regeneration were performed at a constant pressure of 3 bar, as shown in Figure 11. The adsorption capacity is constant from the first to the tenth cycle; the average amount of adsorption in these ten cycles is 2.23 mmol/g, and the standard deviation and variance are 2.9% and 0.08%, respectively. Therefore, there has not been much change in the adsorption amount of each cycle.

Figure 11: Cyclic adsorption/desorption of H_2S on USY zeolite.

Adsorption of hydrogen sulfide on USY is completely regenerable, and the repeatability of tests confirms the validity of the data. USY zeolite has a stable physical and chemical structure in confronting with hydrogen sulfide gas, adsorption occurs physically on it, and the dissociation adsorption has not occurred. To better see the importance of the results of USY, the hydrogen sulfide adsorption was measured by the previous method, but this time on a 13X zeolite as another type of FAU. This is a commercial zeolite that is widely used in various industries, such as the adsorption of mercaptans, disulfides, carbon dioxide, etc. The physical and chemical characteristics of this adsorbent have been tested and are available in Table 9 and Table 10.

Table 9: Specification of 13X zeolite

Table 10: Composition of 13X by XRF test

Six cycles of adsorption and desorption were performed as before method at 3 bar on this adsorbent, which is shown in Figure 12. The amount of H_2S adsorption from an impressive number of 3.83 mmol/g reached 1.99 mmol/g during two adsorption and desorption cycles, which has lost 48% of its initial adsorption capacity and shows that dissociative adsorption has occurred.

Figure 12: cyclic adsorption/desorption of H_2S on commercial 13X zeolite

3.5. Ideal Selectivity

Selectivity is an index for the removal of a component over other adsorbates. The most accurate way to find the selectivity is to use dynamic adsorption calculation by breakthrough tests, but this test is more expensive than static equilibrium adsorption so ideal selectivity can use as a preliminary estimate. Ideal selectivity is based on Ideal Adsorbed Solution Theory (IAST) [59]. Ideal selectivity also called Henry's selectivity and has the following relationship.

$$\alpha_{n.m} = \frac{K_n}{K_m} \tag{9}$$

K_n and K_m are Henry's constants for n and m components, respectively. Henry's constant is an idea for the affinity of the adsorbate to the adsorbent, near zero loading; it is shown as the following relationship

$$\lim_{P \to 0} \frac{q}{P} = K_H \tag{10}$$

Henry's constant for various tested adsorbents in this study is given in Table 7. There are different Henry's constants for different temperatures, so the ideal selectivity varies at different temperatures. The USY adsorption capacity for hydrogen sulfide diminishes with enhancing temperature, however the selectivity of hydrogen sulfide to carbon dioxide increases. This relationship is not valid for hydrogen sulfide compared to other compounds; therefore, there is a challenge in selecting suitable conditions for the adsorption of hydrogen sulfide over carbon dioxide. On the one hand, with increasing temperature, hydrogen sulfide adsorption decreases, but on the other hand, its selectivity increases. Whether the purpose of using this adsorbent is to remove hydrogen sulfide alone or to remove hydrogen sulfide and carbon dioxide together, it can make a difference in choosing the optimal conditions.

The ideal selectivity values of the tested components, relative to each other, at different temperatures are given in Table 11. At different temperatures, the ideal selectivity of hydrogen sulfide over nitrogen and methane is good, but the selectivity over carbon dioxide is close to unity, in general, high values of ideal selectivity are desirable because this leads to sharper separation in fixed bed adsorption devices [60]. The selectivity of hydrogen sulfide and carbon dioxide to methane and nitrogen decreases with increasing temperature.

Table 11: Ideal selectivity of compounds by USY

According to IAST, the reason for increasing the selectivity of hydrogen sulfide to carbon dioxide with temperature is investigated in the adsorption affinity factor. In the Toth adsorption isotherm, the adsorption affinity is indicated by b; this coefficient is shown in Table 7 for different components, the affinity of an adsorbent depends on various factors such as the kinetic diameter of adsorbent, the polarity of adsorbate, the temperature of the system, etc. The adsorption affinity in the Toth model is shown according to the following relationship [41]

$$b = b_\infty exp\left(\frac{Q}{R_g T}\right) \qquad (11)$$

b_∞ *the* constant is the adsorption affinity at unlimited temperature and expresses the effect of various factors on adsorption other than temperature. b_∞ shows how much the molecule is adsorbed on the adsorbent surface [41]. Q is the heat of adsorption, and T is the system's temperature. The affinity is inversely dependent on the temperature; because the adsorption heat is positive, the adsorption affinity decreases with increasing temperature. According to equation (11), the lower heat of adsorption, the lower effect of temperature changes on the affinity.

Table 8 shows that the adsorption heat of carbon dioxide on USY is 63% more than hydrogen sulfide; therefore, the effect of temperature on the affinity of carbon dioxide is greater. As the temperature increases, the rate of decrease in the affinity of carbon dioxide is higher than the rest of the components, which have less adsorption heat; hence, the selectivity of carbon dioxide compared to other components decreases with increasing temperature, and as a result, the H_2S/CO_2 selectivity increases with increasing temperature, the same interpretation is true for the rest of the components.

4. Conclusions

USY zeolite was chosen for the removal of hydrogen sulfide as an important impurity in natural gas. Hydrogen sulfide, methane, carbon dioxide, and nitrogen adsorption isotherms were measured on this zeolite at high pressure. Adsorption of hydrogen sulfide on USY is 4.47 mmol/g at 283K and 12 bar; the maximum possible adsorption was also calculated as 4.93 mmol/g according to Toth's model. Compared to other zeolites, USY exhibits good adsorption in the presence of hydrogen sulfide.

Conventional commercial zeolites, like many surface adsorbents, exhibit dissociative adsorption when exposed to hydrogen sulfide. In this work, it was studied that USY is completely regenerable after adsorbing hydrogen sulfide. During the ten adsorption and regeneration cycles, the adsorption capacity of this adsorbent did not decrease after hydrogen sulfide adsorption. The isosteric adsorption heat of hydrogen sulfide was calculated by the Clausius-Clapeyron method on USY as 18.1 kJ/mol, which indicates the physical adsorption of hydrogen sulfide on the adsorbent.

USY is an FAU-type zeolite; to compare the regeneration ability of USY, a 13X zeolite was selected, which is FAU-type like USY; due to the dissociation of hydrogen sulfide during six cycles of adsorption and regeneration, the adsorption capacity of 13X decreased by 48%.

The ideal selectivity of hydrogen sulfide to carbon dioxide enhanced by raising the temperature. At the same time, the adsorption capacity decreases with increasing temperature. Therefore, if the goal is to remove hydrogen sulfide alone, there is a challenge: higher temperature equals lower adsorption and higher selectivity, but if the simultaneous removal of acid gases (H_2S and CO_2) are involved, and reducing the temperature is beneficial for the adsorption process. Due to the higher adsorption heat of carbon dioxide on USY compared to other components of natural gas, as the temperature increases, its selectivity decreases compared to other compounds.

USY is a high-tech zeolitic adsorbent; according to our study, has a suitable adsorption capacity and complete regeneration in confronting hydrogen sulfide, and can be used for natural gas sweetening.

5. References

[1] T. Yu, Z. Chen, Z. Liu, J. Xu, Y. Wang, Review of Hydrogen Sulfide Removal from Various Industrial Gases by Zeolites, Separations. 9 (2022) 229. https://doi.org/10.3390/separations9090229.

[2] M. Hervy, D. Pham Minh, C. Gérente, E. Weiss-Hortala, A. Nzihou, A. Villot, L. Le Coq, H2S removal from syngas using wastes pyrolysis chars, Chem. Eng. J. 334 (2018) 2179–2189. https://doi.org/10.1016/j.cej.2017.11.162.

[3] H. Förster, M. Schuldt, Infrared spectroscopic study of the adsorption of hydrogen sulfide on zeolites NaA and NaCaA, J. Colloid Interface Sci. 52 (1975) 380–385. https://doi.org/10.1016/0021-9797(75)90213-1.

[4] M. Kheirinik, N. Rahmanian, M. Farsi, M. Garmsiri, Revamping of an acid gas absorption unit: An industrial case study, J. Nat. Gas Sci. Eng. 55 (2018) 534–541. https://doi.org/10.1016/j.jngse.2018.05.016.

[5] A. Pudi, M. Rezaei, V. Signorini, M.P. Andersson, M.G. Baschetti, S.S. Mansouri, Hydrogen sulfide capture and removal technologies: A comprehensive review of recent developments and emerging trends, Sep. Purif. Technol. 298 (2022) 121448. https://doi.org/10.1016/j.seppur.2022.121448.

[6] L. Sigot, G. Ducom, P. Germain, Adsorption of hydrogen sulfide (H2S) on zeolite (Z): Retention mechanism, Chem. Eng. J. 287 (2016) 47–53. https://doi.org/10.1016/j.cej.2015.11.010.

[7] M. Gaillard, V. Montouillout, F. Maugé, C. Fernandez, An infrared and Solid-State NMR study of the H2S adsorption on basic zeolite, in: Microporous Mesoporous Mater., 2004: pp. 1679–1685. https://doi.org/10.1016/S0167-2991(04)80694-3.

[8] J.L.B. de Oliveira, B.O. Nascimento, D.V. Gonçalves, R.G. Santiago, S.M.P. de Lucena, D.C.S. de Azevedo, M. Bastos-Neto, Effect of ultramicropores on the mechanisms of H2S retention from biogas, Chem. Eng. Res. Des. 154 (2020) 241–249. https://doi.org/10.1016/j.cherd.2019.12.019.

[9] H.G. Karge, J. Raskó, Hydrogen sulfide adsorption on faujasite-type zeolites with systematically varied Si-Al ratios, J. Colloid Interface Sci. 64 (1978) 522–532. https://doi.org/10.1016/0021-9797(78)90394-6.

[10] J.H. Yang, Hydrogen sulfide removal technology: A focused review on adsorption and catalytic oxidation, Korean J. Chem. Eng. 38 (2021) 674–691. https://doi.org/10.1007/s11814-021-0755-y.

[11] I. Ferino, R. Monaci, E. Rombi, V. Solinas, L. Burlamacchi, Temperature-programmed desorption of H2S from alkali-metal zeolites, Thermochim. Acta. 199 (1992) 45–55. https://doi.org/10.1016/0040-6031(92)80249-V.

[12] A. Starke, C. Pasel, C. Bläker, T. Eckardt, J. Zimmermann, D. Bathen, Investigation of the Adsorption of Hydrogen Sulfide on Faujasite Zeolites Focusing on the Influence of Cations, ACS Omega. 7 (2022) 43665–43677. https://doi.org/10.1021/acsomega.2c04606.

[13] A. Georgiadis, N. Charisiou, M. Goula, Removal of Hydrogen Sulfide From Various Industrial Gases: A Review of The Most Promising Adsorbing Materials, Catalysts. 10 (2020) 521. https://doi.org/10.3390/catal10050521.

[14] K. Yang, B. Su, L. Shi, H. Wang, Q. Cui, Adsorption Mechanism and Regeneration Performance of 13X for H 2 S and SO 2, Energy & Fuels. 32 (2018) 12742–12749. https://doi.org/10.1021/acs.energyfuels.8b02978.

[15] J. SCHERZER, Ion exchanged ultrastable Y zeolites I. Formation and structural characterization of lanthanum-hydrogen exchanged zeolites, J. Catal. 46 (1977) 100–108. https://doi.org/10.1016/0021-9517(77)90140-3.

[16] H.G. Karge, J. Weitkamp, eds., Adsorption and Diffusion, Springer Berlin Heidelberg, Berlin, Heidelberg, 2008. https://doi.org/10.1007/978-3-540-73966-1.

[17] A.J. Cruz, J. Pires, A.P. Carvalho, M.B. De Carvalho, Physical Adsorption of H2S Related to the Conservation of Works of Art: The Role of the Pore Structure at Low Relative Pressure, Adsorption. 11 (2005) 569–576. https://doi.org/10.1007/s10450-005-5614-3.

[18] D. Crespo, G. Qi, Y. Wang, F.H. Yang, R.T. Yang, Superior Sorbent for Natural Gas Desulfurization, Ind. Eng. Chem. Res. 47 (2008) 1238–1244. https://doi.org/10.1021/ie071145i.

[19] L.H. de Oliveira, J.G. Meneguin, M.V. Pereira, E.A. da Silva, W.M. Grava, J.F. do Nascimento, P.A. Arroyo, H2S adsorption on NaY zeolite, Microporous Mesoporous Mater. 284 (2019) 247–257. https://doi.org/10.1016/j.micromeso.2019.04.014.

[20] M. Ozekmekci, G. Salkic, M.F. Fellah, Use of zeolites for the removal of H 2 S: A mini-review, Fuel Process. Technol. 139 (2015) 49–60. https://doi.org/10.1016/j.fuproc.2015.08.015.

[21] M. Khabazipour, M. Anbia, Removal of Hydrogen Sulfide from Gas Streams Using Porous Materials: A Review, Ind. Eng. Chem. Res. 58 (2019) 22133–22164. https://doi.org/10.1021/acs.iecr.9b03800.

[22] M. Rahmani, B. Mokhtarani, M. Mafi, N. Rahmanian, Acid Gas Removal by Superhigh Silica ZSM-5: Adsorption Isotherms of Hydrogen Sulfide, Carbon Dioxide, Methane, and Nitrogen, Ind. Eng. Chem. Res. 61 (2022) 6600–6610. https://doi.org/10.1021/acs.iecr.2c00196.

[23] S. Tanada, K. Boki, T. Kita, K. Sakaguchi, Adsorption behavior of hydrogen sulfide inside micropores of Molecular Sieve Carbon 5A and Molecular Sieve Zeolite 5A, Bull. Environ. Contam. Toxicol. 29 (1982) 624–629. https://doi.org/10.1007/BF01669632.

[24] A.J. Hernández-Maldonado, R.T. Yang, D. Chinn, C.L. Munson, Partially Calcined Gismondine Type Silicoaluminophosphate SAPO-43: Isopropylamine Elimination and Separation of Carbon Dioxide, Hydrogen Sulfide, and Water, Langmuir. 19 (2003) 2193–2200. https://doi.org/10.1021/la026424j.

[25] X. HU, MULTICOMPONENT ADSORPTION EQUILIBRIUM OF GASES IN ZEOLITE: EFFECT OF PORE SIZE DISTRIBUTION, Chem. Eng. Commun. 174 (1999) 201–214. https://doi.org/10.1080/00986449908912796.

[26] X. Chen, B. Shen, H. Sun, G. Zhan, Ion-exchange modified zeolites X for selective adsorption desulfurization from Claus tail gas: Experimental and computational investigations, Microporous Mesoporous Mater. 261 (2018) 227–236. https://doi.org/10.1016/j.micromeso.2017.11.014.

[27] K.G. Wynnyk, B. Hojjati, P. Pirzadeh, R.A. Marriott, High-pressure sour gas adsorption on zeolite 4A, Adsorption. 23 (2017) 149–162. https://doi.org/10.1007/s10450-016-9841-6.

[28] L. Barelli, G. Bidini, L. Micoli, E. Sisani, M. Turco, 13X Ex-Cu zeolite performance characterization towards H2S removal for biogas use in molten carbonate fuel cells, Energy. 160 (2018) 44–53. https://doi.org/10.1016/j.energy.2018.05.057.

[29] A. Nuhnen, C. Janiak, A practical guide to calculate the isosteric heat/enthalpy of adsorption via adsorption isotherms in metal–organic frameworks, MOFs, Dalt. Trans. 49 (2020) 10295–10307. https://doi.org/10.1039/D0DT01784A.

[30] K.S. Françoise Rouquerol, Jean Rouquerol, Adsorption by Powders and Porous Solids, Elsevier, 1999. https://doi.org/10.1016/B978-0-12-598920-6.X5000-3.

[31] Z. Du, X. Nie, S. Deng, L. Zhao, S. Li, Y. Zhang, J. Zhao, Comparative analysis of calculation method of adsorption isosteric heat: Case study of CO2 capture using MOFs, Microporous Mesoporous Mater. 298 (2020) 6. https://doi.org/10.1016/j.micromeso.2020.110053.

[32] S. Brandani, E. Mangano, L. Sarkisov, Net, excess and absolute adsorption and adsorption of helium, Adsorption. 22 (2016) 261–276. https://doi.org/10.1007/s10450-016-9766-0.

[33] U.O. Wolfgang Wagner, ThermoFluids, 1st ed., Springer Berlin, Heidelberg, 2005.

[34] E.W. Lemmon, R. Span, Short Fundamental Equations of State for 20 Industrial Fluids, J. Chem. Eng. Data. 51 (2006) 785–850. https://doi.org/10.1021/je050186n.

[35] R. Span, W. Wagner, A New Equation of State for Carbon Dioxide Covering the Fluid Region from the Triple-Point Temperature to 1100 K at Pressures up to 800 MPa, J. Phys. Chem. Ref. Data. 25 (1996) 1509–1596. https://doi.org/10.1063/1.555991.

[36] U. Setzmann, W. Wagner, A New Equation of State and Tables of Thermodynamic Properties for Methane Covering the Range from the Melting Line to 625 K at Pressures up to 100 MPa, J. Phys. Chem. Ref. Data. 20 (1991) 1061–1155. https://doi.org/10.1063/1.555898.

[37] R. Span, E.W. Lemmon, R.T. Jacobsen, W. Wagner, A. Yokozeki, A Reference Equation of State for the Thermodynamic Properties of Nitrogen for Temperatures from 63.151 to 1000 K and Pressures to 2200 MPa, J. Phys. Chem. Ref. Data. 29 (2000) 1361–1433. https://doi.org/10.1063/1.1349047.

[38] R.D. McCarty, Vincent D. Arp, A New Wide Range Equation of State for Helium, in: R. W. Fast (Ed.), Adv. Cryog. Eng., Springer, Boston, MA, 1990. https://doi.org/https://doi.org/10.1007/978-1-4613-0639-9_174.

[39] S. V. Gupta, Measurement Uncertainties, Springer Berlin Heidelberg, Berlin, Heidelberg, 2012. https://doi.org/10.1007/978-3-642-20989-5.

[40] J.P. Meyer, M. De Paepe, eds., The Art of Measuring in the Thermal Sciences, CRC Press, 2020. https://doi.org/10.1201/9780429201622.

[41] D.D. Do, Adsorption Analysis: Equilibria and Kinetics, PUBLISHED BY IMPERIAL COLLEGE PRESS AND DISTRIBUTED BY WORLD SCIENTIFIC PUBLISHING CO., 1998. https://doi.org/10.1142/p111.

[42] Jozsef Toth, Adsorption: Theory, Modeling, and Analysis, First edit, Marcel Dekker, 2002.

[43] C.M. HURVICH, C.-L. TSAI, Regression and time series model selection in small samples, Biometrika. 76 (1989) 297–307. https://doi.org/10.1093/biomet/76.2.297.

[44] M.J. Gurka, L.J. Edwards, 8 Mixed Models, in: 2007: pp. 253–280. https://doi.org/10.1016/S0169-7161(07)27008-7.

[45] G. Glatting, P. Kletting, S.N. Reske, K. Hohl, C. Ring, Choosing the optimal fit function: Comparison of the Akaike information criterion and the F-test, Med. Phys. 34 (2007) 4285–4292. https://doi.org/10.1118/1.2794176.

[46] D. Nicholson, T. Stubos, Simulation of Adsorption in Micropores, in: 2000: pp. 231–256. https://doi.org/10.1016/S0927-5193(00)80011-X.

[47] M. Murialdo, N.P. Stadie, C.C. Ahn, B. Fultz, Observation and Investigation of Increasing Isosteric Heat of Adsorption of Ethane on Zeolite-Templated Carbon, J. Phys. Chem. C. 119 (2015) 944–950. https://doi.org/10.1021/jp510991y.

[48] S. Sircar, Basic Research Needs for Design of Adsorptive Gas Separation Processes, Ind. Eng. Chem. Res. 45 (2006) 5435–5448. https://doi.org/10.1021/ie051056a.

[49] K.V. Kumar, S. Gadipelli, C.A. Howard, W. Kwapinski, D.J.L. Brett, Probing adsorbent heterogeneity using Toth isotherms, J. Mater. Chem. A. 9 (2021) 944–962. https://doi.org/10.1039/D0TA08150G.

[50] K.D. Hammond, W.C. Conner, Analysis of Catalyst Surface Structure by Physical Sorption, in:

2013: pp. 1–101. https://doi.org/10.1016/B978-0-12-420173-6.00001-2.

[51] Y. Wang, H. Jia, X. Fang, Z. Qiu, T. Du, CO2 and water vapor adsorption properties of framework hybrid W-ZSM-5/silicalite-1 prepared from RHA, RSC Adv. 10 (2020) 24642–24652. https://doi.org/10.1039/D0RA03736B.

[52] S.H. Madani, S. Sedghi, M.J. Biggs, P. Pendleton, Analysis of Adsorbate-Adsorbate and Adsorbate-Adsorbent Interactions to Decode Isosteric Heats of Gas Adsorption, ChemPhysChem. 16 (2015) 3797–3805. https://doi.org/10.1002/cphc.201500881.

[53] D.D. Do, D. Nicholson, H.D. Do, On the anatomy of the adsorption heat versus loading as a function of temperature and adsorbate for a graphitic surface, J. Colloid Interface Sci. 325 (2008) 7–22. https://doi.org/10.1016/j.jcis.2008.05.027.

[54] V.J. Inglezakis, A.A. Zorpas, Heat of adsorption, adsorption energy and activation energy in adsorption and ion exchange systems, Desalin. Water Treat. 39 (2012) 149–157. https://doi.org/10.1080/19443994.2012.669169.

[55] T.J. Bandosz, On the Adsorption/Oxidation of Hydrogen Sulfide on Activated Carbons at Ambient Temperatures, J. Colloid Interface Sci. 246 (2002) 1–20. https://doi.org/10.1006/jcis.2001.7952.

[56] R. Sadegh-Vaziri, M.U. Babler, Removal of Hydrogen Sulfide with Metal Oxides in Packed Bed Reactors—A Review from a Modeling Perspective with Practical Implications, Appl. Sci. 9 (2019) 5316. https://doi.org/10.3390/app9245316.

[57] X. Liu, R. Wang, Effective removal of hydrogen sulfide using 4A molecular sieve zeolite synthesized from attapulgite, J. Hazard. Mater. 326 (2017) 157–164. https://doi.org/10.1016/j.jhazmat.2016.12.030.

[58] H.G. Karge, M. Ziółek, M. Łaniecki, U.v./vis and i.r. spectroscopic study of hydrogen sulphide adsorption on faujasite-type zeolites, Zeolites. 7 (1987) 197–202. https://doi.org/10.1016/0144-2449(87)90050-9.

[59] A.L. Myers, J.M. Prausnitz, Thermodynamics of mixed-gas adsorption, AIChE J. 11 (1965) 121–127. https://doi.org/10.1002/aic.690110125.

[60] R. Krishna, J.M. van Baten, Elucidation of Selectivity Reversals for Binary Mixture Adsorption in Microporous Adsorbents, ACS Omega. 5 (2020) 9031–9040. https://doi.org/10.1021/acsomega.0c01051.

List of Tables

Table 1: Adsorption of hydrogen sulfide on different zeolitic adsorbents

Zeolite	H_2S Adsorption capacity ($mmol.g^{-1}$)	Reference
High silica ZSM-5	3.04	[22]
5A	2.6	[23]
SAPO-43	1.1	[24]
NaX (13X)	4.8	[17]
4A	2.9	[17]
NaY	4.7	[17]
13X	4.8	[17]

H-mordenite	2.3	[25]
Na-CuY	4	[18]
AgX	1.5	[26]
4A	4.1	[27]
CuX	1.2	[28]

Table 2: weight percentage of the constituent elements of USY

Component	Weight%
O	53.00
Na	0.21
Al	0.84
Si	45.95

Table 3: Specifications of ultra-stable Y Zeolite

Specification	Value	unit
BET $_{surface\ area}$	510.32	(m^2/g)
Total pore volume	0.4314	(cm^3/g)
V_{micro}	0.2764	(cm^3/g)
Pore diameter	1.64	(nm)

Table 4: The statistical model of data fitting

Model		**1.Toth**			**2.Sips**			**3.Langmuir**			**4.Freundlich**		
Temp. (k)		**283**	**293**	**303**	**283**	**293**	**303**	**283**	**293**	**303**	**283**	**293**	**303**
Standard Error:	**H_2S**	0.0483	0.0393	0.0205	0.0468	0.0364	0.0251	0.0901	0.0691	0.0576	0.2817	0.2156	0.1783
R^2		1.000	1.000	1.000	1.000	1.000	1.000	0.999	0.999	0.999	0.986	0.989	0.992
r		0.9992	0.9993	0.9998	0.9993	0.9994	0.9997	0.9970	0.9976	0.9982	0.9730	0.9779	0.9838
AICc		-101.5	-115.0	-138.4	-102.6	-117.7	-131.1	-81.7	-96.1	-102.6	-41.5	-53.7	-60.6
Standard Error:	**CO**	0.0485	0.0280	0.0223	0.0468	0.0311	0.0336	0.0723	0.0582	0.0513	0.2259	0.2542	0.1932

R^2		0.9996	0.9998	0.9998	0.9996	0.9998	0.9996	0.9990	0.9992	0.9991	0.9891	0.9863	0.9881
r		0.9992	0.9997	0.9997	0.9992	0.9996	0.9993	0.9980	0.9985	0.9983	0.9783	0.9728	0.9764
AICc		-125.7	-148.7	-165.9	-127.2	-144.3	-147.9	-110.2	-119.3	-130.6	-64.3	-56.1	-70.9
Standard Error:	**CH_4**	0.0054	0.0065	0.0025	0.0065	0.0052	0.0029	0.0071	0.0080	0.0030	0.0469	0.0311	0.0258
R^2		1.0000	0.9999	1.0000	1.0000	1.0000	1.0000	0.9999	0.9999	1.0000	0.9977	0.9986	0.9987
r		0.9999	0.9999	1.0000	0.9999	0.9999	1.0000	0.9999	0.9998	1.0000	0.9954	0.9973	0.9975
AICc		-228.7	-220.2	-261.7	-220.4	-229.9	-256.2	-217.6	-212.1	-255.0	-133.2	-151.3	-159.4
Standard Error:	**N_2**	0.0010	0.0017	0.0051	0.0015	0.0008	0.0039	0.0040	0.0069	0.0087	0.0115	0.0072	0.0061
R^2		1.0000	1.0000	0.9999	1.0000	1.0000	0.9999	1.0000	0.9998	0.9997	0.9996	0.9998	0.9999
r		1.0000	1.0000	0.9998	1.0000	1.0000	0.9999	0.9999	0.9996	0.9994	0.9993	0.9996	0.9997
AICc		-314.7	-291.3	-219.9	-296.2	-328.5	-231.1	-253.8	-229.0	-199.3	-204.2	-225.7	-213.0

Table 5: Experimental adsorption data of H_2S adsorption on USY

283 K		**293 K**		**303 K**	
P (mbar)	q (mmol/g)	P (mbar)	q (mmol/g)	P (mbar)	q (mmol/g)
0	0.000	0	0.000	0	0.000
54	0.085	138	0.141	48	0.042
194	0.259	468	0.446	186	0.153
430	0.511	722	0.630	448	0.333
750	0.831	1053	0.912	788	0.552
1062	1.147	1404	1.189	1281	0.866
1310	1.427	1747	1.440	1809	1.202
1723	1.826	2106	1.721	2204	1.462
2522	2.485	2522	2.023	2586	1.678
3275	2.921	3042	2.328	3248	2.029
3936	3.207	3708	2.604	4017	2.331
4847	3.476	4678	2.936	4756	2.562
6052	3.746	5623	3.187	5684	2.811
6943	3.913	6365	3.334	6835	3.081
7991	4.091	7588	3.546	8004	3.290
8987	4.237	8769	3.749	9315	3.471
10903	4.410	9828	3.905	10324	3.583
		10947	4.05	11040	3.675
Uncertainties: ΔT= 0.1 K, ΔP=1 mbar, Max. $\Delta q/q$=2%					

Table 6: Experimental adsorption data of CO_2, CH_4 and N_2 adsorption on USY

CO_2						CH_4						N_2					
283 K		293 K		303 K		283 K		293 K		303 K		283 K		293 K		303 K	
P (mbar)	q (mmol/g)	P (mbar)	q (mmol/g)	P (mbar)	q (mmol/g)	P (mbar)	q (mmol/g)	P (mbar)	q (mmol/g)	P (mbar)	q (mmol/g)	P (mbar)	q (mmol/g)	P (mbar)	q (mmol/g)	P (mbar)	q (mmol/g)
0	0.000	0	0.000	0	0.000	0	0.000	0	0.000	0	0.000	0	0.000	0	0.000	0	0.000
86	0.109	46	0.028	64	0.034	58	0.013	79	0.011	57	0.004	72	0.013	67	0.007	77	0.003
161	0.182	135	0.101	168	0.095	161	0.030	166	0.025	247	0.028	177	0.022	151	0.016	179	0.014
307	0.301	416	0.305	536	0.292	337	0.062	354	0.052	388	0.044	221	0.026	338	0.031	528	0.041
524	0.464	591	0.416	832	0.433	573	0.104	644	0.097	602	0.070	549	0.051	584	0.050	1044	0.078
805	0.664	815	0.549	1184	0.574	861	0.153	894	0.129	868	0.097	973	0.083	923	0.075	1530	0.117
1123	0.890	1165	0.739	1501	0.701	1234	0.210	1284	0.177	1243	0.139	1270	0.107	1262	0.099	2023	0.149
1476	1.144	1538	0.939	2140	0.945	1667	0.275	1663	0.236	1657	0.183	1639	0.137	1708	0.134	2862	0.200
2025	1.528	2098	1.228	2869	1.217	2264	0.362	2297	0.317	2293	0.248	2261	0.184	2264	0.172	3728	0.250
2608	1.910	2731	1.546	3644	1.494	2921	0.454	2964	0.392	3001	0.317	2960	0.236	3088	0.227	5065	0.327
3364	2.314	3481	1.889	4246	1.685	3893	0.583	3778	0.480	4009	0.411	3956	0.306	3860	0.281	5856	0.369
4440	2.727	4652	2.326	4804	1.857	4964	0.715	4984	0.604	5035	0.503	5219	0.39	4371	0.315	6926	0.424
5544	3.004	5684	2.614	5597	2.048	5921	0.830	6048	0.710	5887	0.576	6230	0.453	5126	0.360	7869	0.473
6366	3.199	6408	2.776	6482	2.268	6873	0.931	6875	0.796	6901	0.659	7057	0.504	5983	0.411	8970	0.528
8388	3.498	8317	3.099	7527	2.457	8598	1.103	7749	0.894	7714	0.720	8188	0.571	6986	0.468	10431	0.598
9900	3.661	9996	3.289	8430	2.606	10314	1.265	8838	0.988	8884	0.811	8876	0.61	7720	0.509	11895	0.665
11828	3.845	11954	3.499	9843	2.778	12232	1.406	10584	1.124	10556	0.926	10591	0.705	8965	0.576	13992	0.759
13860	4.026	13720	3.667	11915	2.996	13561	1.501	12364	1.253	12291	1.043	12411	0.8	10615	0.661	15555	0.824
15972	4.183	15880	3.819	13510	3.136	15662	1.634	14553	1.396	14210	1.156	13973	0.879	12473	0.753	16836	0.875
18414	4.313	18032	3.927	15961	3.290	16996	1.706	16320	1.494	16409	1.274	16306	0.99	14668	0.855	19801	0.991
20382	4.410	20419	4.046	17949	3.381	19194	1.817	18711	1.611	18879	1.389	17889	1.06	16487	0.936	20862	1.031
				20514	3.498	20628	1.871	20884	1.715	20883	1.475	19847	1.145	18914	1.037		
												20954	1.19	20818	1.113		
Uncertainties: ΔT= 0.1 K, ΔP=1 mbar, Maximum $\Delta q/q$=2.2%																	

Table 7: Toth model parameters, Henry's constant (K_H)

adsorbent	H_2S			CO_2			CH_4			N_2		
T(K)	**283**	**293**	**303**	**283**	**293**	**303**	**283**	**293**	**303**	**283**	**293**	**303**
q_m	4.93	4.68	4.33	4.85	4.58	4.04	-	-	-	-	-	-
b	0.25	0.20	0.17	0.19	0.15	0.12	0.05	0.035	0.034	0.01	0.009	0.005
t	1.63	1.58	1.72	1.35	1.42	1.53	1.17	0.81	1.11	0.62	0.61	0.49
K_H	1.21	0.95	0.73	0.92	0.68	0.49	0.17	0.17	0.11	0.09	0.09	0.09

Table 8: the heat of adsorption on USY

Component	The heat of Adsorption (-ΔH) (kJ/mol)
H_2S	18.1 ± 0.5
CO_2	22.5 ± 0.6
CH_4	14.6 ± 0.7
N_2	3.6 ± 0.2

Table 9: Specification of 13X zeolite

Test	Result	Test Method
Phase	Faujsite	XRD
BET, Surface Area (m^2/g)	679	ISO 9277
Total Pore Volume (m^3/g)	0.29	ISO 15901
Average Pore Diameter (nm)	1.7	ISO 15901
Loss of attrition (mass%)	<1	ASTM D4058
Moisture content @ 230°C, 3hr (mass%)	<0.1	BS 3482-2
L.O.I @ 950°C, 1hr (mass%)	0.8	UOP 954

Table 10: composition of 13X by XRF test

composition	mass%
SiO_2	46.9
$A_{l2}O_3$	29.5
Fe_2O_3	1.8
CaO	0.1
Na_2O	15.8
K_2O	0.1
MgO	3
TiO_2	0.1
MnO	0.1
P_2O_3	1
SO_3	1

Table 11: Ideal selectivity of compounds by USY

Selectivity	283 (K)	293 (K)	303 (K)
H_2S/CO_2	1.3	1.4	1.5
H_2S/CH_4	7.1	5.7	6.5
H_2S/N_2	13.2	12.1	8.0

CO_2/CH_4	5.4	4.1	4.3
CO_2/N_2	10.0	6.8	5.4
CH_4/N_2	1.9	1.7	1.2

List of Figures

Figure 9: Adsorption isotherms on USY at 283K; red circles, H_2S; green squares, CO_2; orange triangles, CH_4; blue tilted squares, N_2; dashed line, Toth model.

Figure 10: trend of isosteric adsorption heat of CO_2, H_2S, CH_4 and N_2 on USY.

Figure 11: Cyclic adsorption/desorption of H_2S on USY zeolite.

Figure 12: Cyclic adsorption/desorption of H_2S on commercial 13X zeolite

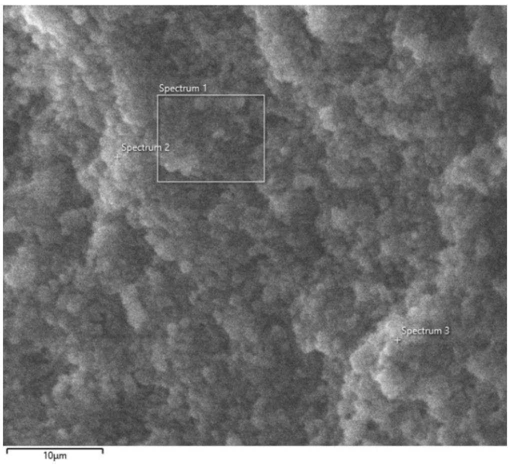

Figure 1: SEM image of USY surface.

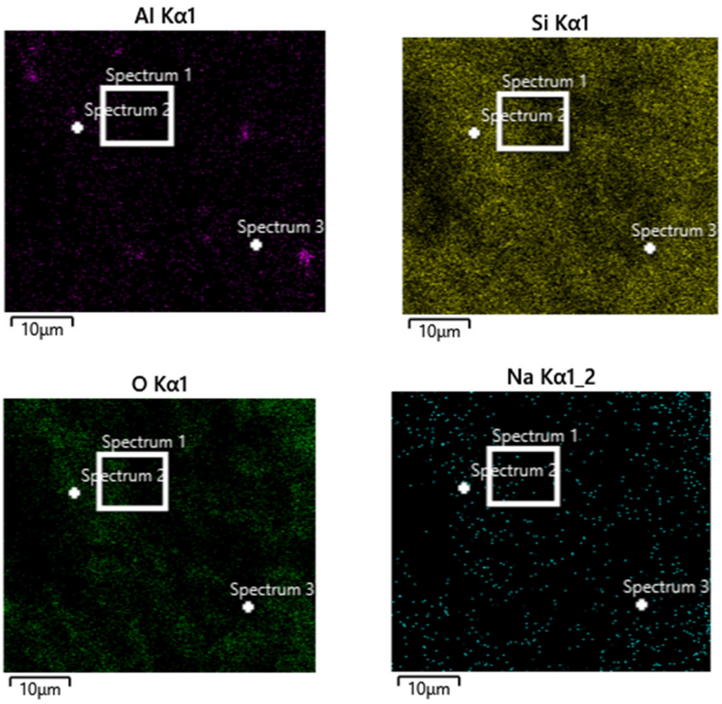

Figure 2: distribution of Na, Si, Al, and O atoms on USY

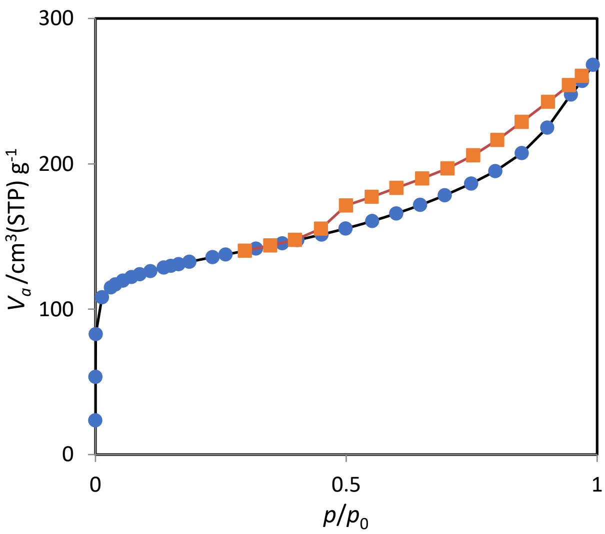

Figure 3: Adsorption-Desorption isotherm of nitrogen on the USY; circles, adsorption; squares, desorption.

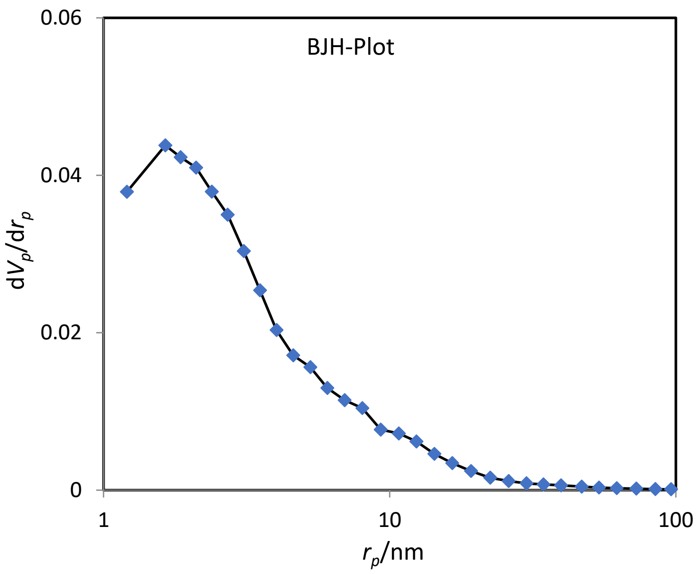

Figure 4: Pore size distribution of ultra-stable Y Zeolite

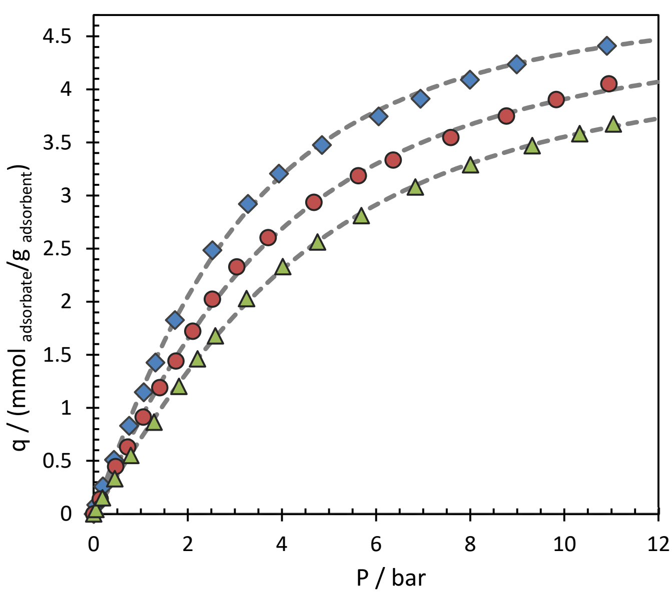

Figure 5: H_2S adsorption isotherms on USY; blue tilted squares, 283K; red circles, 293K; green triangles, 303K; dashed lines, Toth model.

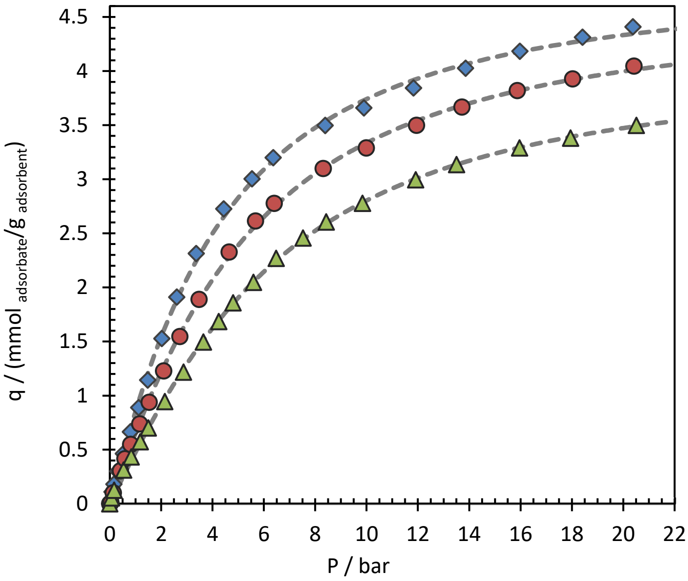

Figure 6: CO_2 adsorption isotherms on USY; blue tilted squares, 283K; red circles, 293K; green triangles, 303K; dashed lines, Toth model.

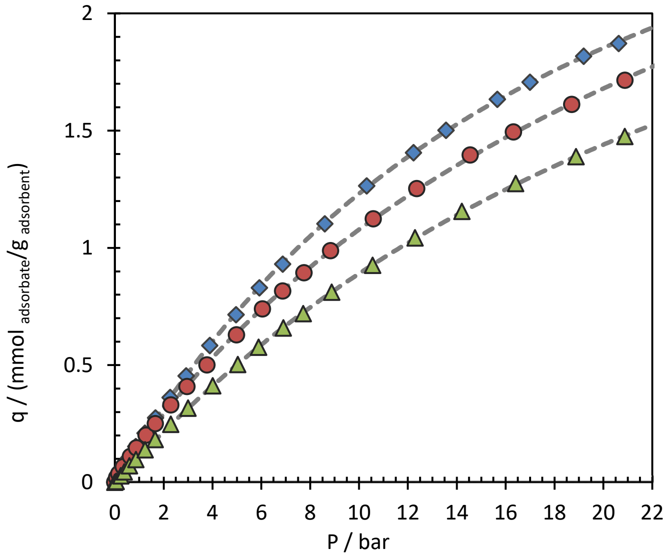

Figure 7: Methane adsorption isotherms on USY; blue tilted squares, 283K; red circles, 293K; green triangles, 303K; dashed lines, Toth model.

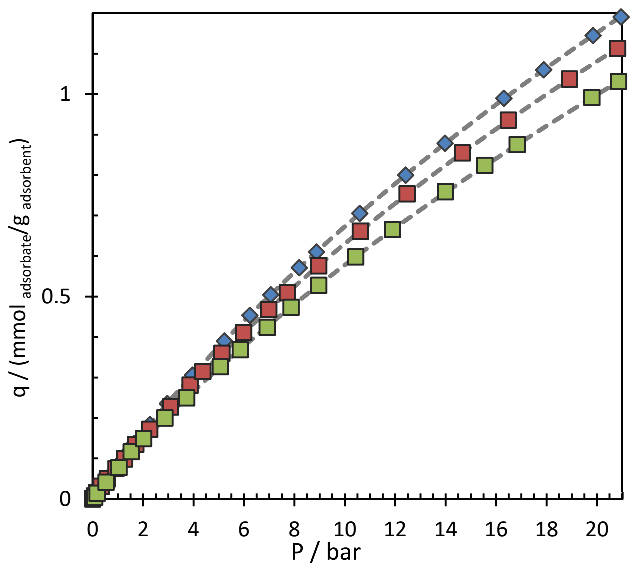

Figure 8: Nitrogen adsorption isotherms on USY; blue tilted squares, 283K; red circles, 293K; green triangles, 303K; dashed lines, Toth model.

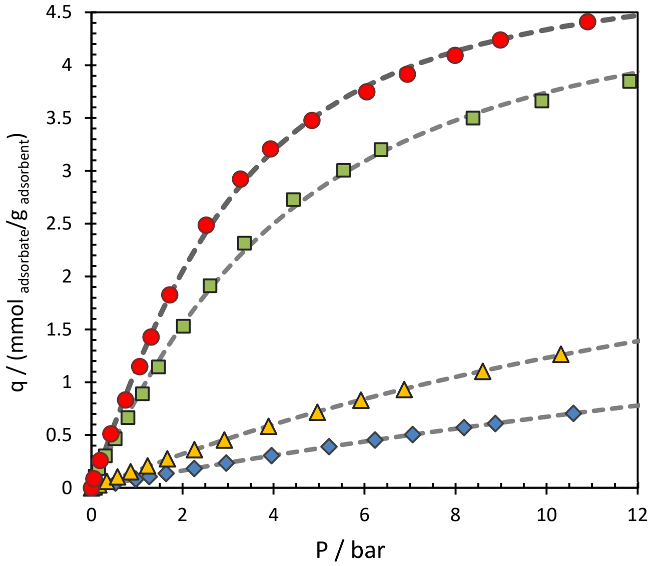

Figure 9: Adsorption isotherms on USY at 283K; red circles, H_2S; green squares, CO_2; orange triangles, CH_4; blue tilted squares, N_2; dashed line, Toth model.

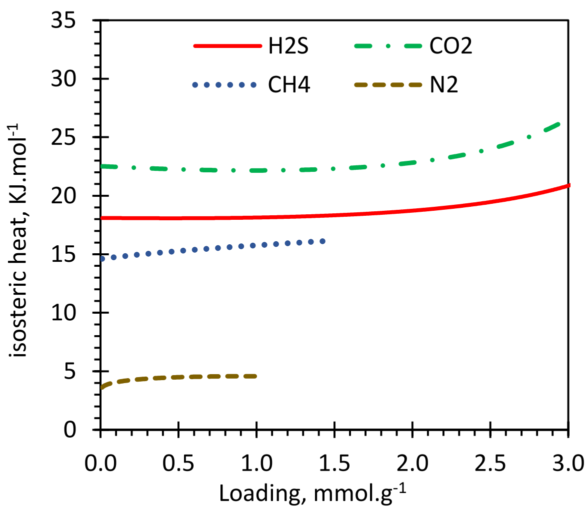

Figure 10: trend of isosteric adsorption heat of CO_2, H_2S, CH_4 and N_2 on USY.

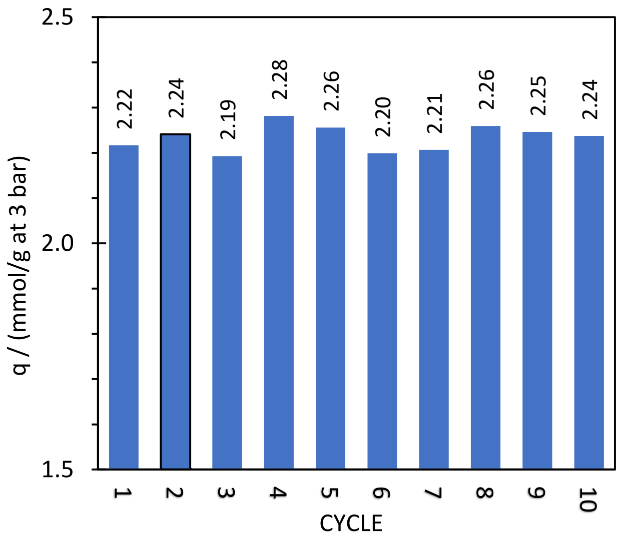

Figure 11: Cyclic adsorption/desorption of H_2S on USY zeolite.

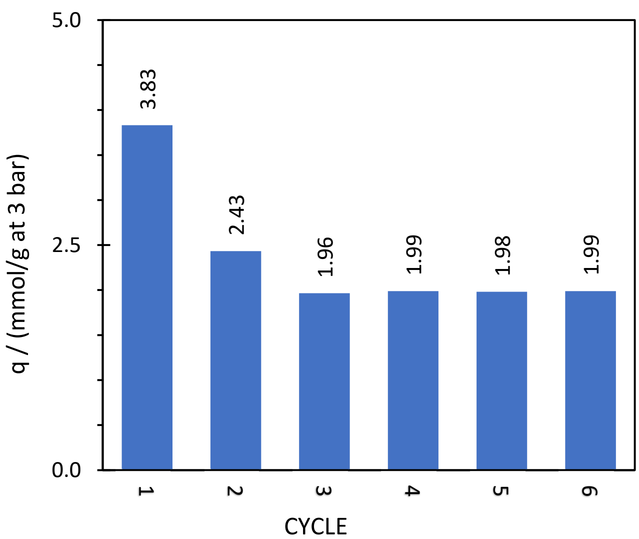

Figure 12: Cyclic adsorption/desorption of H_2S on commercial 13X zeolite

Graphical Abstract: